applied optics

Multiregion apodized photon sieve with enhanced efficiency and enlarged pinhole sizes

Tao Liu, Xin Zhang,* Lingjie Wang, Yanxiong Wu, Jizhen Zhang, and Hemeng Qu

Key Laboratory of Optical System Advanced Manufacturing Technology, Changchun Institute of Optics and Fine Mechanics and Physics, Chinese Academy of Sciences, Changchun 130033, China
**Corresponding author: optlab@ciomp.ac.cn*

Received 8 May 2015; revised 30 June 2015; accepted 20 July 2015; posted 20 July 2015 (Doc. ID 240616); published 11 August 2015

A novel multiregion structure apodized photon sieve is proposed. The number of regions, the apodization window values, and pinhole sizes of each pinhole ring are all optimized to enhance the energy efficiency and enlarge the pinhole sizes. The design theory and principle are thoroughly proposed and discussed. Two numerically designed apodized photon sieves with the same diameter are given as examples. Comparisons have shown that the multiregion apodized photon sieve has a 25.5% higher energy efficiency and the minimum pinhole size is enlarged by 27.5%. Meanwhile, the two apodized photon sieves have the same form of normalized intensity distribution at the focal plane. This method could improve the flexibility of the design and the fabrication the apodized photon sieve.

OCIS codes: (050.0050) Diffraction and gratings; (050.1940) Diffraction; (050.1965) Diffractive lenses; (110.0110) Imaging systems; (350.1260) Astronomical optics.

http://dx.doi.org/10.1364/AO.54.007175

1. INTRODUCTION

The photon sieve (PS), a new kind of diffractive optical element, was first proposed by Kipp [1] based on a traditional Fresnel zone plate. Research [1–5] has shown that the size of the pinholes (d) can be increased beyond the underlying zone width (w) by a factor of 1.53, 3.51, 5.51, and so on while still maintaining constructive interference. This character is utilized to relax the fabrication requirements for the PS. Due to its important applications in high-resolution microscopy, spectroscopy, x-ray or EUV lithography, and ultralarge membrane photon sieve telescopes, a lot of research has been done in terms of resolution, energy efficiency, and sidelobe suppression [6–11].

Some theoretical analysis and experimental results showed that the enlargement of the sizes of uniformly distributed pinholes in annular ring regions by a factor of $d/w = 1.53, 3.51, 5.51$ will not affect their own normalized complex amplitude distribution in the focal region at the focal plane [12]. The only influence is the energy efficiency. Inspired by the above discussions, the pinhole ring diffraction model for the focusing analysis of the photon sieve was developed in [13]. According to the pinhole ring diffraction model, all of the uniformly distributed pinholes in a ring zone could be treated as a single unity when investigating the focusing property. Then the diffracted field of the individual pinhole ring could be given. In terms of the linear superposition principle, the diffracted fields of the pinhole rings could be further summed up to analyze the focusing property of the whole PS at a fast speed.

In this paper, we propose a novel multiregion apodized PS (MAPS) designed with the pinhole ring diffraction model in the framework of a scalar field. Figure 1 shows the schematic views of one classic apodized PS and the MAPS. The classic apodized PS utilizes an apodization window for the pinhole density modulation in each ring. As for the MAPS, it is divided into different annular regions. The number of regions, the apodization window values, and size of the pinholes can be optimized for the MAPS. In Section 2, the comprehensive influences of the above three factors on the diffracted field of the MAPS are given. We denote d_m as the diameter of the pinhole in the mth ring, and w_m as the width of the mth ring zone. Our investigation also reveals that the highest energy efficiency for the individual pinhole ring could be achieved when the ratio $d_m/w_m = 1.17$, instead of the commonly used $d_m/w_m = 1.53$. Based on the calculations and analysis, the design theory and principle of the MAPS are thoroughly discussed and proposed. In Section 3, we numerically designed one classic apodized PS and one two-region MAPS. Comparisons have been done between the two apodized PS examples of focal lengths of 175 mm and diameters of 30 mm at a working wavelength of 632.8 nm. The investigation shows that the MAPS has better performance in terms of higher energy efficiency and enlarged pinhole sizes. Meanwhile, the two PSs have the same normalized intensity distributions at the focal plane. Finally, we conclude our discussions in Section 4. This design method may give rise to new ideas for the design of the

1559-128X/15/247175-06$15/0$15.00

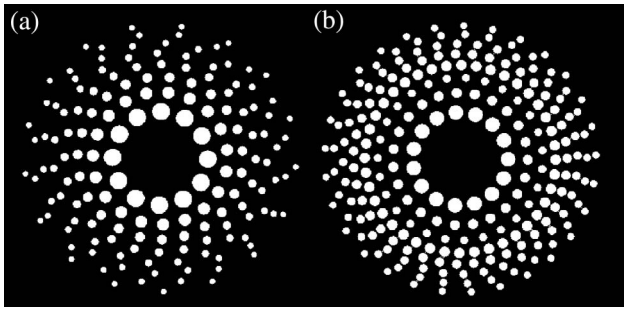

Fig. 1. Schematic illustration showing the pattern of (a) a classic apodized PS and (b) a multiregion apodized PS.

apodized photon sieve and put forward the development of the photon sieve.

2. DESIGN THEORY

As shown in Fig. 2, the photon sieve is perpendicularly illuminated by a collimated incident light beam with unit amplitude. The distance from the PS plane to the image plane is the focal length f. We denote r_n as the distance from the center of the nth circular pinhole in the mth ring to the center of the PS. Those circular pinholes in the mth ring have the same semidiameter a_n and are distributed uniformly in angle in the ring zone. Now let us discuss the rotationally symmetric diffracted field $U_m(R)$ for the mth pinhole ring which is composed of N_m circular pinholes. The focal spot for a PS is usually quite small, which means R is quite small compared with r_n. When investigating the diffracted field of the small focal region, it has been shown in Ref. [13] that all of the pinholes in a ring zone could be treated as a single unity. It means instead of analyzing individual pinholes, we could evaluate the focusing of the pinhole ring within the pinhole ring diffraction model. According to the pinhole ring diffraction model, if the Fresnel number of those pinholes $N_f = \pi a_n^2/(\lambda f) \le 0.05$, $R/r_n \le 0.05$, and $N_m \ge 100$, the analytical expression for the overall diffractive field of the uniformly distributed pinholes in the mth ring can be given as

$$U_m(R) = N_m \frac{kA_n a_n^2 f}{H_0^2} Jinc\left(\frac{ka_n}{H_0} r_n\right) \exp(jkH_0) J_0\left(\frac{kRr_n}{H_0}\right), \quad (1)$$

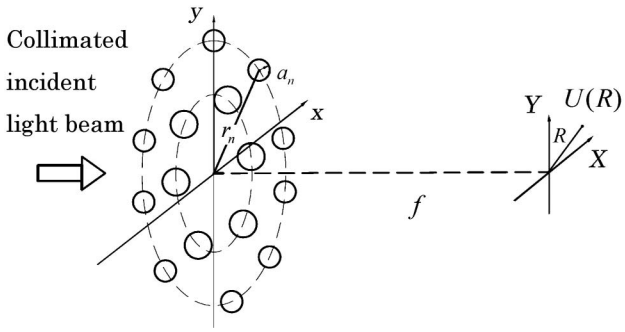

Fig. 2. Schematic view of a general PS with collimated incident light beam.

where $Jinc(\cdot) = J_1(\cdot)/(\cdot)$, $J_1(\cdot)$ is the first-order Bessel function, A_n is the constant real amplitude in the nth pinhole, j is the imaginary unit, $k = 2\pi/\lambda$ is the wave number, and $H_0 = (f^2 + R^2 + r_n^2)^{1/2}$.

Equation (1) is Eq. (13) of Ref. [13] and we quote it here for our starting point. According to the linear superposition principle, the total diffracted field at the image plane for the PS can be calculated by the summation of those individual diffracted fields. It also can be seen from Eq. (1) that the complex diffracted field of the individual pinhole ring is influenced by both of the parameters N_m and a_n.

Now we analyze the relationship between the diffracted field of all of the pinholes in a ring zone and the apodization parameters. Note that the pinholes in the mth ring have the same size and are distributed uniformly in angle in the same ring zone. Thus, it is more convenient to substitute the subscript n in the above expressions by m. Then A_n, a_n, and r_n would be transformed into A_m, a_m, and r_m. Let us investigate the value of $H_0 = (f^2 + R^2 + r_m^2)^{1/2}$. Since the quantity R^2 is far smaller than the quantity $f^2 + r_m^2$, we can further replace the three H_0 in the dominators of Eq. (1) by $f_m = (f^2 + r_m^2)^{1/2}$. Substituting the above approximation and transforms into Eq. (1), one can immediately obtain that

$$U_m(R) = N_m \frac{A_m d_m f}{2 f_m r_m} J_1\left(\frac{\pi}{2}\frac{d_m}{w_m}\right) \exp(jkH_0) J_0\left(\frac{kRr_m}{f_m}\right), \quad (2)$$

where $d_m = 2a_m$ and $w_m = \lambda f_m/(2r_m)$. The subscript m in d_m and w_m means that these two values may vary in our following discussion of the MAPS. It is obvious that each circular pinhole subtends a small angle of d_m/r_m from the center of the PS. Then the value of N_m can be given by

$$N_m = C_m \frac{2\pi}{d_m/r_m}, \quad (3)$$

where C_m is a density factor for the mth ring to keep the interval of those pinholes. The parameter C_m must be in the range of $0 \le C_m \le 1.0$, and $C_m = 1.0$ is the maximum case when the pinholes are located one by one without an interval. We define the density factor C_m as the initial ratio of the total number of pinholes to the number of the maximum case. Strictly speaking, there are tiny differences between the actual pinhole number N_m and the value calculated by $C_m 2\pi/(d_m/r_m)$. That is because the value will be rounded so as to get an integer pinhole number N_m in each ring. Substituting Eq. (3) into Eq. (2), one can obtain

$$U_m(R) = C_m \frac{\pi A_m f}{f_m} J_1\left(\frac{\pi}{2}\frac{d_m}{w_m}\right) \exp(jkH_0) J_0\left(\frac{kRr_m}{f_m}\right). \quad (4)$$

It is well known that apodization could be easily incorporated into a PS by modifying the pinhole density of each ring zone with an apodization window. A lot of work has been done concerning the suppression of sidelobes with different apodization windows. We denote $G(r)$ as the apodization window implemented to modulate the pinhole density in each ring. Then the pinhole number in the apodized mth ring is changed to

$$N_{mG} = G(r_m) C_m \frac{2\pi}{d_m / r_m}. \quad (5)$$

After pinhole density apodization, the corresponding diffracted field of all the pinholes sitting in the mth ring could be changed into

$$U_{mG}(R) = C_m G(r_m) \frac{\pi A_m f}{f_m} J_1\left(\frac{\pi}{2}\frac{d_m}{w_m}\right) \exp(jkH_0) J_0\left(\frac{kRr_m}{f_m}\right). \quad (6)$$

Equation (6) is the analytical expression for the diffracted field of the apodized individual pinhole ring. It clearly shows that the diffracted light field was influenced by both of the two factors: the apodization window value $G(r_m)$ and the ratio factor d_m/w_m. It also provides theoretical explanations for the finding in Ref. [12] that the change of ratio d_m/w_m in the annular ring regions will not affect the normalized complex amplitude distribution in the focal region.

Then let us focus on the diffracted field value at the focal point where $R = 0$. Equation (6) can be further reduced into

$$U_{mG}(0) = C_m G(r_m) \frac{\pi A_m f}{f_m} J_1\left(\frac{\pi}{2}\frac{d_m}{w_m}\right) \exp(jkf_m). \quad (7)$$

When the apodization window value $G(r_m)$ is determined, one can immediately get the following expression

$$U_{mG}(0) \propto J_1\left(\frac{\pi}{2}\frac{d_m}{w_m}\right). \quad (8)$$

Let us compare Eq. (8) with Eq. (16) in Ref. [2] which deals with the focusing contribution of an individual pinhole and is expressed as $U_n(0,0) \propto (d/w) J_1[\pi d/(2w)]$. Despite the subscript difference, the main difference between these two equations is a factor of d_m/w_m. This can be explained as follows. As can be seen from Eq. (3), the total number of pinholes N_m in a ring zone is related to the diameter d_m of the pinholes. By treating all of the uniformly distributed pinholes in a ring zone as a single unity, the factor d_m/w_m is eliminated during the calculation of the overall pinhole ring focusing contribution.

Figure 3 shows the change of the field value $U_{mG}(0)$ with the increase of the ratio factor d_m/w_m. It can be found that the relative maximum values of $|U_{mG}(0)|$ appear when $d_m/w_m \approx$ 1.17, 3.40, 5.44, 7.45, and so on. It is interesting to compare Fig. 3 with the curve in Fig. 2 of Ref. [2] and Fig. 2 of Kipp's Ref. [1]. We can see that although the ratio d_m/w_m for a single pinhole is 1.53, 3.51, 5.51, 7.51, and so on for the relative maximum diffraction contribution to the desired focal point ($R = 0$), they are not the best solutions facing the total contribution of all the pinholes in one ring. The main reason is that a smaller d_m/w_m factor means an increase in the number of pinholes N_m in the ring zone according to Eq. (3). This can be schematically illustrated by the first ring zone in Figs. 1(a) and 1(b). Obviously, the first ring zone in the MAPS has more pinholes than the first ring zone in the classic apodized PS. Thus, more incident light energy would be diffracted to focus at the focal point. In conclusion, by taking the contribution of all of those pinholes into consideration, the optimum ratio factor is $d_m/w_m = 1.17$. This would lead to the highest energy efficiency at the focal point.

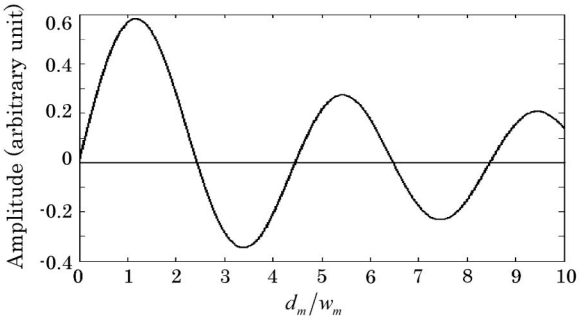

Fig. 3. Analytical description of the field value change of the mth ring $U_{mG}(0)$ with the increase of the ratio d_m/w_m.

While $d_m/w_m = 1.17$ could lead to smaller sized pinholes in the apodized PS, one should keep in mind that the focusing properties of the apodized pinhole rings are modulated by both $G(r_m)$ and d_m/w_m according to Eq. (6). So the problem could be solved by dividing the apodized PS into several regions. In the innermost region, the ratio factor $d_m/w_m = 1.17$ is kept. In the outer regions, larger ratio factors d_m/w_m are taken so as to relax the fabrication requirements. With the substitution of the enlarged d_m/w_m values into Eq. (6), the apodization window values in these outer ring zones are optimized to meet the apodization matching condition. Thus, the corresponding diffracted field would stay unchanged before and after the optimization. The optimized apodization window values should be changed into

$$G'(r_m) = \frac{J_1\left(\frac{\pi}{2} \times 1.17\right) G(r_m)}{J_1\left(\frac{\pi}{2}\frac{d_m}{w_m}\right)}, \quad (9)$$

for the pinhole rings in the outer regions. It is worth mentioning that the values of $G(r_m)C_m$ and $G'(r_m)C_m$ should be smaller than 1.0 to prevent the overlapping of pinholes in the individual ring zone. Then the pinhole numbers in each ring of the optimized MAPS can be calculated by

$$N'_{mG} = G'(r_m) C_m \frac{2\pi}{d_m / r_m}. \quad (10)$$

To this end, the design process of the multiregion apodized photon sieve could be given. First, the initial apodization window $G(r)$ is chosen to modulate the pinhole density in each ring. Second, the apodized PS is divided into several annular regions. The ratio factor d_m/w_m is chosen to be 1.17 for pinholes in the innermost region so as to obtain the maximum total diffraction contribution to the focal point. The third step is crucial. During the third step, the ratio factors d_m/w_m are increased for pinholes in the outer regions. The corresponding optimized apodization window values for individual pinhole rings could be calculated by Eq. (9). Last but not the least, the pinhole numbers for each ring zone could be given by Eq. (10). Then the design of the multiregion apodized photon sieve is complete.

3. NUMERICAL DESIGN EXAMPLES AND ANALYSIS

Now we numerically design two apodized photon sieves: one is the classic Gaussian apodized photon sieve (GAPS) and the

other the optimized MAPS. Both of them have the same aperture of $D = 30$ mm, focal length of 175 mm, and working wavelength of 632.8 nm. The two initial density factors C_m for both of the two PSs are chosen to be 1.0. The pinholes of both of the two photon sieves are all located in the white zones with ring order $m = 1$–1014. The GAPS modulates the pinhole density of each ring zone with a Gaussian window, which could be mathematically described by

$$G(r) = \alpha \exp\left[-\frac{(r-\gamma)^2}{\beta^2}\right]. \tag{11}$$

The triplet Gaussian parameters α, β, and γ are parameters which determine the desired distribution and are selected as (1, $D\sqrt{0.5}/2$, 0) here. The ratio factor d_m/w_m is taken as the commonly used 1.53 for all the pinholes of the classic GAPS. As for the MAPS, it is divided into two regions. In the inner region, the ratio factor d_m/w_m is chosen to be 1.17 and the same Gaussian window values are utilized. In the outer region, the ratio factor d_m/w_m is chosen to be 2.0. This means that the diameter of the pinhole equals to the sum of the underlying white zone and the black zone. This could maximize the pinhole sizes and greatly relax the fabrication requirements of the apodized PS. Then we investigate the boundary between the $d_m/w_m = 1.17$ and $d_m/w_m = 2.0$ regions. Under Eq. (9), the prerequisites for the validity of the mutiregion apodized photon sieve have been shown, which are $G(r_m)C_m \le 1.0$ and $G'(r_m)C_m \le 1.0$. These conditions guarantee that there is no overlapping of pinholes in the individual ring zone. Note that the initial density factor $C_m = 1.0$. So the prerequisite conditions are changed into $G(r_m) \le 1.0$ and $G'(r_m) \le 1.0$ for our numerical examples. It is obvious that the Gaussian window $G(r_m) \le 1.0$ for the classic GAPS. As for the inner region of the MAPS where $d/w = 1.17$, according to Eq. (9) the requirement $G'(r_m) \le 1.0$ is certainly satisfied because $G(r_m) \le 1.0$. For the rest of the pinhole rings in the outer region of the MAPS, by substituting $d_m/w_m = 2.0$ and the Gaussian window values $G(r_m) = \exp[-r_m^2/(D\sqrt{0.5}/2)^2]$ into Eq. (9), the optimized apodization window values can be solved. It can be calculated that the pinhole ring radius r_m should be smaller than 8.97 mm so as to guarantee that $G'(r_m) \le 1.0$. The corresponding ring order is $m = 363$. Thus, in the inner region there are ring orders $m = 1$–363 with $d_m/w_m = 1.17$, and in outer region $m = 364$–1014 with $d_m/w_m = 2.0$. In the end, the pinhole numbers of each ring zone in the two regions are calculated using Eq. (10).

Note that the design for the MAPS is not unique, because one has many parameters that can be used. The number of regions, the apodization window values, and the ratio factor d_m/w_m could all be utilized for the optimization. By dividing the inner region of the above two-region MAPS example into more regions, some of the pinholes could have bigger sizes. However, the peak intensity could not be increased anymore. That is because the ratio factor d_m/w_m in the innermost ring zone is already set as 1.17 and the apodization window values and pinhole sizes in other ring zones are chosen to meet the apodization matching condition. It should be reemphasized that one should carefully choose the apodization parameters to ensure that the relation $G(r_m)C_m \le 1.0$ and $G'(r_m)C_m \le 1.0$ are satisfied. This can be clearly illustrated in Fig. 4(a) which shows the apodization window values of the two PSs. Since the initial density factor $C_m = 1.0$, it can be seen that all of the apodization window values $G(r_m)$ and $G'(r_m)$ are smaller than 1.0. The sizes of the pinholes are plotted in Fig. 4(b). Figure 4(b) clearly illustrates that the sizes of the pinholes in the classic GAPS monotonously decrease with the increase in the pinhole ring radius. The smallest pinhole size is in the outermost ring of the classic GAPS and the diameter is 5.67 μm. As for the optimized two-region MAPS, there is a jump at the boundary between the $d_m/w_m = 1.17$ and $d_m/w_m = 2.0$ regions. The jump is related to the change of the density and size of pinholes during the design of the MAPS. It can be seen from Fig. 4(b) that the diameter of pinholes in ring order $m = 1$–363 of the MAPS are smaller than that in the classic GAPS. However, the pinholes in ring order $m = 364$–1014 of the MAPS have bigger diameters than that in the classic GAPS. This could improve the flexibility of fabricating the apodized PS since pinholes in the outer zones usually have smaller sizes compared with the inner zones. Analysis shows that the smallest pinhole size for the optimized two-region MAPS is 7.23 μm, which is 27.5% bigger than the smallest pinhole size in the classic GAPS.

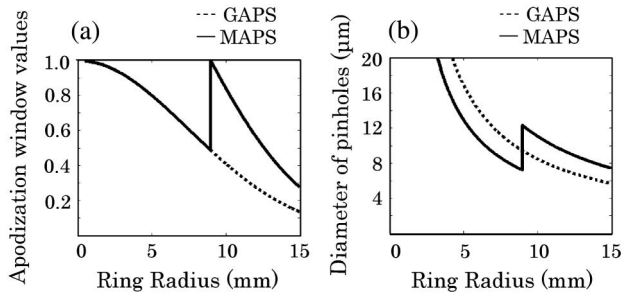

Fig. 4. Comparison of (a) apodization window values and (b) pinhole diameters between the classic GAPS and the optimized MAPS.

It is worth mentioning that the pinhole numbers for the six innermost pinhole rings of this classic GAPS and the four innermost pinhole rings of this two-region MAPS do not meet the requirement $N_m \ge 100$. So the diffracted fields of those few pinhole rings could not be computed using the pinhole ring model equation [Eq. (1)]. Instead they are calculated using Eq. (8) in Ref. [3] which is the nonparaxial far-field model for individual pinholes. Despite this slight inconsistency with the pinhole ring diffraction model, the pinhole numbers in the 10 pinhole rings are still calculated using Eqs. (5) and (10). Investigation shows that the influence of this slight inconsistency is quite small on the overall diffracted field.

To get a better understanding of the difference of the classic GAPS and MAPS, the profiles of part of the two photon sieves within ring order $m = 357$–370 are plotted in Figs. 5(a) and 5(b), respectively. Figure 5(b) clearly demonstrates the change of pinhole sizes and intensity within the boundary region of the MAPS. It can be seen that the ring zones in the MAPS have more pinholes than the corresponding ring zones in the classic GAPS. As is also shown, the pinholes in the outer region of the MAPS have bigger sizes than the corresponding ring zones in the classic GAPS.

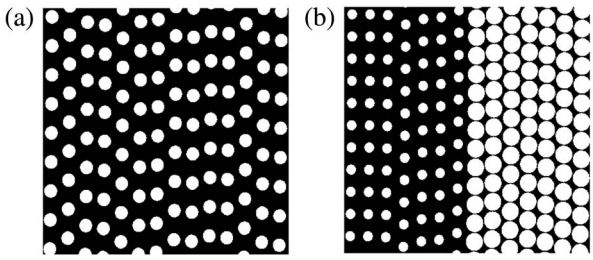

Fig. 5. Profiles of part of (a) the classic GAPS and (b) the optimized two-region MAPS within ring order $m = 357$–370.

The calculated intensity distributions and the normalized intensity distributions along the X axis on the focal plane are illustrated in Figs. 6(a) and 6(b) for the two photon sieves. In Fig. 6(a), the intensities are normalized to the peak intensity of the classic GAPS. It can be seen from Fig. 6(a) that the peak intensity of the optimized MAPS is improved by 25.5%. It means that a higher energy efficiency of 25.5% has been achieved for the two-region MAPS. As a comparison, Fig. 6(b) clearly shows that the normalized intensity distributions of the two photon sieves matched extremely well and the difference is unobservable. These comparisons validate the design theory of the multiregion apodized photon sieves. It should be emphasized that we only discussed intensity distributions near the focal region of the two photon sieves. The intensity distributions are sure to be different for regions far away from the focal point at the focal plane. However, these differences are unimportant because the far away diffracted fields would be blocked by the optical system apertures and could not enter the imaging system.

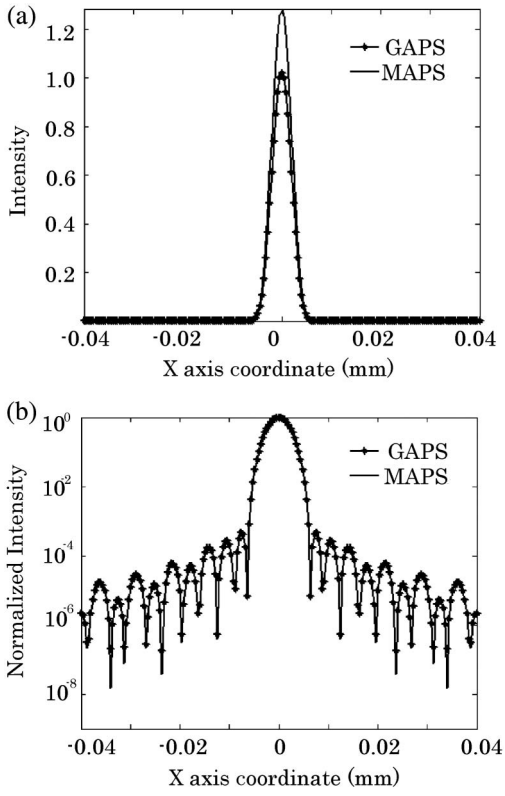

Fig. 6. Comparison of (a) the intensity distribution and (b) the normalized intensity distribution on the focal plane between the classic GAPS and the optimized two-region MAPS. The intensities in (a) are normalized to the peak intensity of the classic GAPS. The intensities in (b) are normalized to the individual peak intensity.

In summary, the optimized MAPS would have the same resolution as the classic GAPS since the apertures of the two apodized photon sieves are the same. Meanwhile, higher energy efficiency could be achieved for the optimized MAPS. In addition, the MAPS with enlarged pinhole sizes would reduce the cost and difficulties of fabricating microstructure pinholes. On the other hand, one could design and manufacture a larger aperture apodized PS under the same limitation of the smallest manufacturable feature. In such case, the larger aperture PS would have higher resolution and higher peak intensity at the focal plane.

4. CONCLUSION

In conclusion, what we believe to be a novel method for the design of a multiregion apodized photon sieve is presented. It has been shown that the number of regions, the apodization window values, and pinhole sizes of each pinhole ring could all be utilized during the design of the apodized PS. Considering the diffraction contributions from all the pinholes in a ring zone, we found that the optimum pinhole size is $d_m/w_m = 1.17$ which could give the highest energy efficiency. The design theory and principle for the multiregion apodized photon sieve are demonstrated within the framework of a scalar field. Two numerical designed examples, one is the classic Gaussian apodized photon sieve and the other the two-region MAPS, are given. Detailed comparisons between the two apodized photon sieves show that the energy efficiency has been increased by 25.5% and the minimum pinhole size enlarged by 27.5% for the MAPS. Meanwhile, the normalized intensity distributions of the two apodized photon sieves, having the same aperture, matched extremely well. We also further elaborated that within the same limitation of the smallest manufacturable features, it is possible to design and manufacture a larger aperture apodized PS. Then higher resolution and higher peak intensity at the focal plane could both be achieved. It is worth mentioning that although we did our example investigation concerning the Gaussian apodized PS, the conclusions could be extended to other apodized PSs. The proposed method and results could give rise to new degrees of freedom for the design of apodized photon sieves by increasing the energy efficiency and the resolution and relaxing the fabrication requirements.

REFERENCES

1. L. Kipp, M. Skibowski, R. L. Johnson, R. Berndt, R. Adelung, S. Harm, and R. Seemann, "Sharper images by focusing soft x-rays with photon sieve," Nature **414**, 184–188 (2001).
2. Q. Cao and J. Jahns, "Focusing analysis of the pinhole photon sieve: individual far field model," J. Opt. Soc. Am. A **19**, 2387–2393 (2002).
3. Q. Cao and J. Jahns, "Nonparaxial model for the focusing of high-numerical-aperture photon sieves," J. Opt. Soc. Am. A **20**, 1005–1012 (2003).
4. G. Andersen, "Large optical photon sieve," Opt. Lett. **30**, 2976–2978 (2005).
5. G. Anderson and D. Tullson, "Broadband antihole photon sieve telescope," Appl. Opt. **46**, 3706–3708 (2007).

6. R. Menon, D. Gil, G. Barbastathis, and H. I. Smith, "Photon-sieve lithography," J. Opt. Soc. Am. A **22**, 342–345 (2005).
7. G. Cheng, C. Hu, P. Xu, and T. Xing, "Zernike apodized photon sieves for high-resolution phase-contrast x-ray microscopy," Opt. Lett. **35**, 3610–3612 (2010).
8. C. Xie, X. Zhu, and J. Jia, "Focusing properties of hard x-ray photon sieves: three-parameter apodization window and waveguide effect," Opt. Lett. **34**, 3038–3040 (2009).
9. C. Xie, X. Zhu, L. Shi, and M. Liu, "Spiral photon sieves apodized by digital prolate spheroidal window for the generation of hard-x-ray vortex," Opt. Lett. **35**, 1765–1767 (2010).
10. A. Sabatyan and S. Mirzaie, "Efficiency-enhanced photon sieve using Gaussian/overlapped distribution of pinholes," Appl. Opt. **50**, 1517–1522 (2011).
11. A. Sabatyan and P. Roshaninejad, "Super-resolving random-Gaussian apodized photon sieve," Appl. Opt. **51**, 6315–6318 (2012).
12. Z. Chen, C. Wang, D. Pu, J. Hu, and L. Chen, "Ultra-large multi-region photon sieves," Opt. Express **18**, 16279–16288 (2010).
13. T. Liu, X. Zhang, L. Wang, Y. Wu, J. Zhang, and H. Qu, "Fast and accurate focusing analysis of large photon sieve using pinhole ring diffraction model," Appl. Opt. **54**, 5327–5331 (2015).